CVI
Journals.ASM.org

Increasing the Potency of an Alhydrogel-Formulated Anthrax Vaccine by Minimizing Antigen-Adjuvant Interactions

Allan Watkinson,[a]* Andrei Soliakov,[b] Ashok Ganesan,[c] Karie Hirst,[d] Chris LeButt,[e] Kelly Fleetwood,[f] Peter C. Fusco,[d] Thomas R. Fuerst,[d] Jeremy H. Lakey[b]

PharmAthene UK Ltd., Billingham, United Kingdom[a]; Institute for Cell and Molecular Biosciences, Faculty of Medical Sciences, University of Newcastle, Newcastle-upon-Tyne, United Kingdom[b]; XstalBio Ltd., Glasgow, United Kingdom[c]; PharmAthene, Inc., Annapolis, Maryland, USA[d]; Defence Science and Technology Laboratory, Porton Down, Salisbury, United Kingdom[e]; Quantics, Edinburgh, United Kingdom[f]

Aluminum salts are the most widely used vaccine adjuvants, and phosphate is known to modulate antigen-adjuvant interactions. Here we report an unexpected role for phosphate buffer in an anthrax vaccine (SparVax) containing recombinant protective antigen (rPA) and aluminum oxyhydroxide (AlOH) adjuvant (Alhydrogel). Phosphate ions bind to AlOH to produce an aluminum phosphate surface with a reduced rPA adsorption coefficient and binding capacity. However, these effects continued to increase as the free phosphate concentration increased, and the binding of rPA changed from endothermic to exothermic. Crucially, phosphate restored the thermostability of bound rPA so that it resembled the soluble form, even though it remained tightly bound to the surface. Batches of vaccine with either 0.25 mM (subsaturated) or 4 mM (saturated) phosphate were tested in a disease model at batch release, which showed that the latter was significantly more potent. Both formulations retained their potency for 3 years. The strongest aluminum adjuvant effects are thus likely to be via weakly attached or easily released native-state antigen proteins.

To combat infectious diseases, subunit vaccines, which consist of a recombinant antigen and an immune-stimulating adjuvant, are increasingly important. These vaccines provide a safer alternative to using live attenuated/inactivated microorganisms or partially purified microbial extracts, while still promoting protective immunity in individuals (1). Currently under development is an anthrax subunit vaccine (SparVax) for anthrax pre- and post-exposure prophylactic treatment. It uses a recombinant protein component, i.e., recombinant protective antigen (rPA), of the anthrax tripartite toxin (2) as the target antigen for toxin-specific neutralizing antibody production. rPA is a relatively poor immunogen by itself, and it needs to be formulated with an adjuvant to provide protection against anthrax infection. In line with several recombinant protein subunit vaccines (3), an aluminum-based adjuvant was chosen, since these mineral adjuvants have been shown to be highly effective and, having been administered to millions of people, have an extensive safety record. The selected adjuvant was Alhydrogel, which is essentially aluminum oxyhydroxide (AlOH) and, with a net positive surface charge, is known to bind to acidic proteins such as rPA (pI 5.6) (4).

The mechanism by which aluminum salts act as adjuvants for vaccine antigens has recently been intensively investigated at the cellular level. Originally they were considered to act simply as a depot maintaining local antigen concentrations (5), but now there are many observations that suggest that more-subtle effects lead to increased protection (6). These effects include NLRP3 inflammasome activation, prostaglandin production, release of endogenous danger signals such as uric acid or DNA following cell death, binding to membrane lipids, and B cell priming (6, 7). In a series of papers, Hansen and colleagues showed that the strength of antigen adsorption to an aluminum-containing adjuvant is inversely related to the immune response (8–10). They also showed that antigens do not need to be bound to the aluminum salt in order to benefit from the adjuvant effect (11) and that interstitial fluid can contribute to dissociation of the antigen-adjuvant complex in newly formulated vaccines but less so in older samples (12). Recently, it was demonstrated that aluminum-adjuvanted antigen dissociates readily from the adjuvant and removal of the injection site and associated alum depot 2 h after injection does not impair the immune response, which raises questions regarding the role of Alhydrogel in forming a stable antigen depot and of the physical interactions between antigen and adjuvant (13). Therefore, we wished to determine if the physical behavior of different formulations of a clinically relevant antigen-Alhydrogel complex had any correlation with short- or long-term potency.

Structurally, Alhydrogel consists of fine crystalline particles made of corrugated layers of aluminum oxyhydroxide (14). Each aluminum atom is coordinated by four oxygen atoms and two hydroxyl groups (15), the layers are held together by hydrogen bonds, and in aqueous solutions, the particles form aggregates ranging from 1 to 10 μm in diameter (16). Nonmodified Alhydrogel particles have a point of 0 charge, i.e., the pH at which the charge on the colloidal particle is 0, of approximately 11. Therefore, Alhydrogel is positively charged at physiological pH and spontaneously adsorbs acidic proteins by an electrostatic attraction mechanism (17). Mixing the rPA protein with the Alhydrogel

Received 17 May 2013 **Returned for modification** 12 July 2013
Accepted 16 August 2013
Published ahead of print 28 August 2013
Address correspondence to Jeremy H. Lakey, jeremy.lakey@ncl.ac.uk.
* Present address: Allan Watkinson, GSB Pharma, Guisborough, United Kingdom.
A.W. and A.S. contributed equally to this article.
Supplemental material for this article may be found at http://dx.doi.org/10.1128/CVI.00320-13.

doi:10.1128/CVI.00320-13

adjuvant at the appropriate concentrations readily, and very rapidly, yields the rPA-Alhydrogel (rPA-AlOH) complex (18).

Structural studies have shown that Alhydrogel-bound proteins, including rPA, preserve their secondary (19, 20), tertiary (18), and quaternary (21, 22) structures but exhibit decreased thermal stability, compared to their free counterparts in solution (23, 24). At the surfaces of adjuvant particles, bound proteins form a monolayer in which individual biomolecules are packed closely together, with no apparent preference for any particular surface orientation. Moreover, the size of protein-adjuvant particles appears to be similar to that of adjuvant particles alone (22, 25) and thus particle aggregation is not a feature of the process.

In addition to the rPA-AlOH complex, the formulation contained two excipients, i.e., (i) saline at physiological levels was included in the formulation to ensure that the anthrax vaccine was isotonic, for recipient comfort upon injection, and (ii) phosphate ions were included with the initial intention of providing buffering capacity. However, it is well established that phosphate groups ligand exchange with aluminum oxyhydroxide, resulting in modification of the surface properties of the colloidal particles (26). For this subunit vaccine formulation, the immediate concern is that the ligand-exchange reaction modifies the point of 0 charge to such an extent that the acidic recombinant protein becomes desorbed from the aluminum oxyhydroxide surface, resulting in high levels of unbound antigen with potential effects on the subsequent immune response. Furthermore, removing a phosphate ion from solution and replacing it with a hydroxyl group has the potential to modify the pH of the formulation. Indeed, it has also been shown that the pH microenvironment adjacent to the aluminum oxyhydroxide particle surface is approximately 2 pH units higher than that of the surrounding solution (27). Since antigen binding occurs in a monolayer at the surface of the aluminum oxyhydroxide particle (22), the antigen will reside in this microenvironment and be subject to conditions different from those of the bulk solution.

As discussed above, Wittayanukulluk and coworkers (27) showed phosphate to be a modifying agent for aluminum oxyhydroxide, due to the effects of the ligand-exchange reaction, in addition to its role as a buffer. Furthermore, by modifying the physical nature of the aluminum oxyhydroxide, phosphate may also affect the potency of any vaccine when it is used as an adjuvant.

Since phosphate constitutes the physiological buffering agent of the anthrax vaccine, we have studied the effects of phosphate ions on the rPA-AlOH formulation. The aims of these studies were to understand the effects of phosphate on the rPA-AlOH colloidal particles, the structure of the protein antigen, the stability of the formulation, and most importantly the potency of the rPA-AlOH vaccine. The data demonstrate that both surface-bound and free phosphate ions have subtle effects on the firmly bound rPA, causing it to behave like a soluble protein. This in turn results in an enhanced immune response, which helps to explain why the adsorption coefficient of rPA-AlOH binding is inversely related to potency (10).

MATERIALS AND METHODS

rPA-Alhydrogel formulation. All chemicals and reagents were purchased from either Sigma-Aldrich (United Kingdom) or Melford Laboratories (United Kingdom), unless otherwise stated. Recombinant protective antigen (rPA) was manufactured by current good manufacturing practices by Avecia Biologics (Billingham, United Kingdom). rPA was expressed as inclusion bodies using *Escherichia coli* strain UT5600(DE3)/pET29a. After solubilization with urea, the protein was refolded by dilution and then purified using anion-exchange and hydrophobic interaction chromatography. The highly purified rPA was then buffer exchanged into phosphate-buffered saline by diafiltration (28), and the concentration was adjusted to give ~1.5 mg/ml. Aliquots of protein were stored at −80°C until required. Aluminum hydroxide gel adjuvant (Alhydrogel) was purchased from either Brenntag Biosector (Denmark) or Sigma-Aldrich (United Kingdom).

rPA was adsorbed to Alhydrogel adjuvant by adding the protein solution to the adjuvant suspension at ambient temperature. Unless otherwise stated, the rPA-AlOH formulations contained 200 μg/ml rPA, 2.6 mg/ml Alhydrogel, 0.9% NaCl, and 0.04% Tween 20 (pH 7.0), with differing concentrations of phosphate. rPA concentrations were measured as absorbance at 280 nm (A_{280}), using an extinction coefficient of 1.176 AU per mg/ml to give the concentration of rPA in solution in mg/ml, by using quartz cuvettes with 1-cm path lengths (Hellma, Germany) in a UV-1800 UV-visible spectrophotometer (Shimadzu, Japan).

Alhydrogel phosphate titration. Phosphate buffer (0 to 5 μmol) was added to 3 mg of Alhydrogel in 1 ml water and vortex mixed. The samples were incubated for 1 h with agitation at ambient temperature and then were centrifuged for 1 min at 20,000 × *g*. The supernatant was then analyzed for phosphate using a colorimetric assay (51); 400 μl of sample was added to 1,200 μl of reagent mixture (100 mM zinc acetate, 15 mM ammonium molybdate [pH 5.0]), vortex mixed, and allowed to react for 1 min before absorbance was measured at 350 nm in a UV-1800 UV-visible spectrophotometer (Shimadzu, Japan), using quartz cuvettes with 1-cm path lengths (Hellma, Germany). Values were calibrated against a phosphate standard curve of NaH_2PO4/Na_2HPO_4 (pH 7.0) containing 0 to 700 μM phosphate.

rPA Langmuir adsorption isotherms. rPA was combined with Alhydrogel in phosphate buffer (0 to 50 mM), and the samples were incubated for 1 h at ambient temperature, with gentle agitation. Subsequently, all samples were centrifuged for 5 min at 14,600 × *g* using a benchtop centrifuge, and rPA concentrations in the supernatant were assessed by measuring A_{280}. The amount of rPA adsorbed to Alhydrogel was calculated by subtracting the rPA remaining in solution from the total added. The adsorption coefficient (K) and the binding capacity (Γ_{max}) were obtained by linearizing the Langmuir equation (10, 29) and were determined using 1/y-axis intercept and 1/slope, respectively.

Zeta potential measurements. The zeta potential was determined using a Zetasizer (Malvern, United Kingdom). One-milliliter samples of rPA-AlOH were introduced into the DTS1060 capillary cells and preequilibrated at 20°C for 2 min prior to electrokinetic analysis, according to the manufacturer's instructions. The zeta potential was automatically determined by the Zetasizer software, using the Smoluchowski equation. Samples were tested in triplicate, with an average of 6 readings per sample.

Circular dichroism. Conventional circular dichroism (CD) becomes inaccurate with particulates that settle and with highly scattering solutions (30). To avoid these problems, we used a solid-state CD technique reported previously, which reduces the effects of light scattering and protein aggregation by the use of a specialized rotating sample cell holder (31). The raw data were corrected for protein concentration and converted into differential extinction coefficient ($\Delta\varepsilon$) units (M^{-1} cm^{-1}) by using the molar concentration of amino acid residues for far-UV CD data and the molar concentration of rPA for near-UV data. The spectra were measured in triplicate from freshly prepared independent samples.

Intrinsic tryptophan fluorescence. Tryptophan fluorescence was measured at ambient temperature using a Cary Eclipse spectrofluorometer (Agilent, United Kingdom) with an excitation wavelength of 280 nm; the emission spectra were measured between 300 and 400 nm. rPA-Alhydrogel samples were measured directly in quartz cuvettes with 1-cm path lengths (Hellma, United Kingdom). To prevent sedimentation and to maintain the homogeneity of the suspended rPA-Alhydrogel particles, samples were stirred using a small magnetic stirring bar placed inside the

cuvette. Data were comparable to those obtained from front-face illumination of a triangular cuvette, but stirring was more reliable in the standard square-footprint design.

In order to provide more-accurate evaluation of the emission spectra, the barycentric mean (the center of an integrated emission curve) was determined using the equation $\lambda_m = (\Sigma F_\lambda \times \lambda)/\Sigma F_\lambda$, where λ_m is the barycentric mean, λ is the wavelength, and F_λ is the point fluorescence at wavelength λ (32). Thermal denaturation was monitored via tryptophan fluorescence using a Cary Eclipse spectrofluorometer equipped with a temperature controller and quartz cuvettes with 1-cm path lengths (Hellma, United Kingdom) with plastic lids. A small magnetic stirring bar inside the cuvette stirred the sample while the temperature was increased from 25°C to 65°C at a rate of 1°C min^{-1}. The variation of fluorescence (F) with increasing temperature (T) was measured using wavelengths of 280 nm for excitation and 340 nm for emission. The transition temperature was determined as the peak value of the first-order derivative dF/dT.

Calorimetry. Differential scanning calorimetry measurements were made using a VP-DSC microcalorimeter (MicroCal, United Kingdom). Prior to analysis, all samples were degassed in a ThermoVac unit (MicroCal, United Kingdom). Samples of rPA-Alhydrogel with 0.3 mg/ml rPA and 3 mg/ml phosphate-saturated Alhydrogel in either 0, 1, 5, 10, 20, or 50 mM free phosphate were analyzed. Samples were scanned between 25°C and 60°C at the rate of 1°C min^{-1}, and Alhydrogel diluted in the formulation buffer was used as a reference. Scans were not completely reversible, and thus the quantitative thermodynamic interpretation is limited. The data were simply processed using MicroCal Origin software to obtain the protein melting temperature (T_m) and, from the area under the peak, enthalpy (ΔH). Isothermal titration calorimetry (ITC) was conducted in a VP-ITC titration microcalorimeter (MicroCal, United Kingdom). All samples were equilibrated by dialysis against the same buffer (150 mM NaCl [pH 7.0]) and degassed as described above. The Alhydrogel suspension was placed in the stirred chamber (300 rpm) and the rPA solution in the syringe. Titration was performed with injection volumes of 10 μl for 20 s, injection spacing of 200 s, cell temperature of 25°C, and reference power of 15 μcal/s. The ITC data were processed, including subtraction of reference scans (rPA into buffer) from sample scans, with Origin software.

Mouse anthrax challenge assay. The mouse anthrax challenge assay, which emulates the human immunological response to anthrax infection, was used for all release and stability testing of the rPA vaccine. All investigations involving animals were carried out according to the requirements of the United Kingdom Home Office legislation and the Animals (Scientific Procedures) Act of 1986. Potency was determined using a mouse challenge assay with a single immunization followed by subsequent challenge with anthrax STI spores. Female A/J mice (Harlan Laboratories, United Kingdom), between 7 and 12 weeks of age, were injected with either test rPA-AlOH vaccine (either 0.25 mM phosphate or 4 mM phosphate) or a freshly formulated reference standard containing rPA-AlOH. During immunization, each dose was administered in a total volume of 0.1 ml, in two 0.05-ml aliquots administered intramuscularly from the same syringe into each hind limb. Both the reference and test items were administered as two parallel 4-point dilution series with doses ranging between 0.2 and 0.004 μg/ml, with 15 mice/dose. The mice were transferred to an Advisory Committee on Dangerous Pathogens (ACDP) level III isolator for spore challenge. At day 21 following the single immunization, each mouse was challenged with 2×10^6 *Bacillus anthracis* STI spores administered intraperitoneally (range of 0.9×10^6 to 5×10^6 spores), which is equivalent to 2,000 times the median lethal dose. All immunizations and spore challenges were performed by a single operator. Following the spore challenge, all animals were closely monitored for up to 8 days, and the time to death was recorded. Humane endpoints were strictly observed for animals showing signs of disease.

Potency was determined using a survival model that describes the relationship between vaccine concentration and mouse survival, and 50% effective dose (ED_{50}) values were determined. In this study, the ED_{50} is the estimated concentration at which 50% of the mice survive to 8 days. For a single material, the predictor is the $\log_{10}$ vaccine concentration and the response is the number of days survived by each mouse. For mice that survive until day 8, the survival time is censored, i.e., the model takes into account the fact that the mice are alive on the final day of the test. With this model, the survival time is assumed to follow a log-normal distribution, which means that the logarithm of survival time follows a normal distribution.

For a single material, the following parameters are defined for each concentration i ($i = 1, 2, 3,$ or 4): C_i, the vaccine concentration for group i; N_i, the number of mice challenged for group i (N_i is usually 15); S_{ij}, the number of days the jth mouse from group i survived, where $j = 1, 2, \ldots, N_i$. S_{ij} is censored at 8 days.

The survival model for a given material can be expressed as $E(\log_e S) = \alpha + (\beta \times \log_{10} C)$. The equation describes a straight line with slope β and intercept α. Once α and β have been estimated, it is possible to calculate the ED_{50} of the material. For a log-normal distribution, this is equivalent to the concentration at which the mean log survival time is $\log_e 8$. At the ED_{50}, we have $\log_e 8 = \alpha + (\beta \times \log_{10} ED_{50})$, $\log_{10} ED_{50} = (\log_e 8 - \alpha)/\beta$, and $ED_{50} = 10^{(\log_e 8 - \alpha)/\beta}$. The variance of $\log_{10} ED_{50}$ can be approximated using the Taylor series method, i.e., $\mathrm{var}[\log_{10} ED_{50}] = (1/\beta^2)[\mathrm{var}(\alpha) + 2 \times \mathrm{cov}(\alpha,\beta) \times \log_{10} ED_{50} + \mathrm{var}(\beta) \times (\log_{10} ED_{50})^2]$.

Long-term stability determination. The stability of each of the materials was investigated using weighted linear regression. Each estimate of $\log ED_{50}$ was weighted by the inverse of the variance of the estimate, such that precise estimates were given more weight than imprecise estimates. The weighted linear regression produces a line of best fit to the data, such that the intercept provides an estimate of the $\log ED_{50}$ at manufacture and the slope provides an estimate of the change in the $\log ED_{50}$ per month. A P value was calculated for the slope, indicating whether the $\log ED_{50}$ changed over time. All analysis was conducted using R statistical software (version 2.12.1 for Windows).

RESULTS

Phosphate titration of Alhydrogel. The saturation curve of phosphate binding to Alhydrogel was determined in the absence of rPA. All added phosphate bound to the Alhydrogel until the saturation point was reached, when residual free phosphate appeared in the supernatant. It was evident from the binding curve that, for 1.5 mg of Alhydrogel in 1 ml, saturation was reached when 0.65 μmol of phosphate had bound (phosphate concentration of around 1 mM in this experiment). This gives a saturation level of 0.43 μmol of phosphate per mg of Alhydrogel (Fig. 1).

Langmuir adsorption isotherms. The ligand-exchange reaction introduces negative charge to the surface of Alhydrogel; to characterize the effect on rPA-Alhydrogel interactions, we determined the strength of binding (adsorption coefficient) and the binding capacity by fitting data to a Langmuir adsorption isotherm (10, 29). This analysis was performed with both nonmodified and phosphate-saturated Alhydrogel. When it was observed that rPA still bound to phosphate-saturated Alhydrogel, we extended the analysis to examine the effects of free phosphate on the protein-adjuvant interactions. The concentrations of free phosphate tested were between 0 and 50 mM. In Langmuir analysis, the strength of binding is given by the adsorption coefficient, with higher adsorption coefficient values indicating stronger interactions. For nonmodified Alhydrogel, rPA had an adsorption coefficient of 215 ml/mg. This value substantially decreased in the presence of phosphate (Fig. 2A). Similarly, there was a sharp reduction in the binding capacity (Fig. 2B). Both the adsorption coefficient and the binding capacity were further reduced by free phosphate, before reaching a steady state at around 5 to 10 mM phosphate.

To evaluate directly the effects of phosphate on the normal

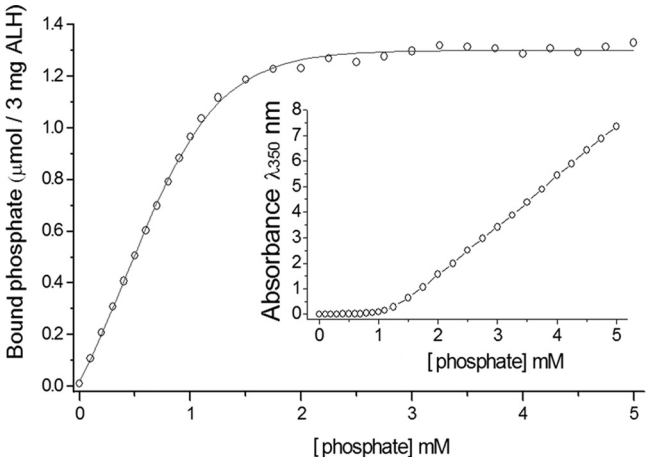

FIG 1 Saturation curve for binding of phosphate to Alhydrogel (ALH). These data were fitted to the Boltzmann sigmoid equation using nonlinear regression analysis in Origin software (version 7.5; OriginLab Corp.). (Inset) Raw absorbance data obtained in the spectrophotometric phosphate assay.

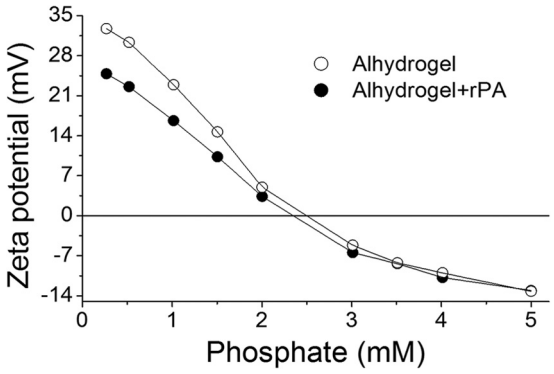

FIG 3 Zeta potentials. Curves demonstrate the effects of phosphate on the zeta potential of Alhydrogel with and without rPA.

vaccine formulation, rPA at 200 μg/ml was formulated with 2.6 mg/ml Alhydrogel at increasing concentrations of phosphate, and the level of unbound rPA was determined using UV absorbance (Fig. 2C). As expected, when the phosphate levels were increased, the levels of unbound rPA correspondingly increased. Whereas the unbound rPA content remained below 5% with 5 mM phosphate, the content increased to around 12% with 10 mM phosphate.

Zeta potential measurements. Changes in the Alhydrogel surface charge (zeta potential) as a function of phosphate concentration were measured using a Zetasizer Nano ZS system (Malvern). The analysis was performed with Alhydrogel (2.6 mg/ml) alone and with 200 μg/ml rPA bound to 2.6 mg/ml Alhydrogel, with increasing concentrations of phosphate. As expected from previous studies (33), the zeta potential of Alhydrogel was positive at physiological pH. With increasing phosphate saturation, the potential rapidly declined and eventually become negative (Fig. 3), with a point of 0 charge at 2.5 mM phosphate. Alhydrogel with adsorbed rPA exhibited similar changes; however, the initial zeta potential of Alhydrogel with bound rPA was lower than that of Alhydrogel alone and the point of 0 charge was at 2.3 mM phosphate. This initial difference was attributed to the negative charge on the adsorbed protein. The zeta potential values for Alhydrogel and rPA-AlOH converged around 3.5 mM.

Isothermal titration calorimetry of rPA binding to Alhydrogel. The modified adjuvant was prepared by treating Alhydrogel with phosphate to produce saturation levels of 10, 50, and 100%, according to the phosphate saturation curve in Fig. 1. Titration of

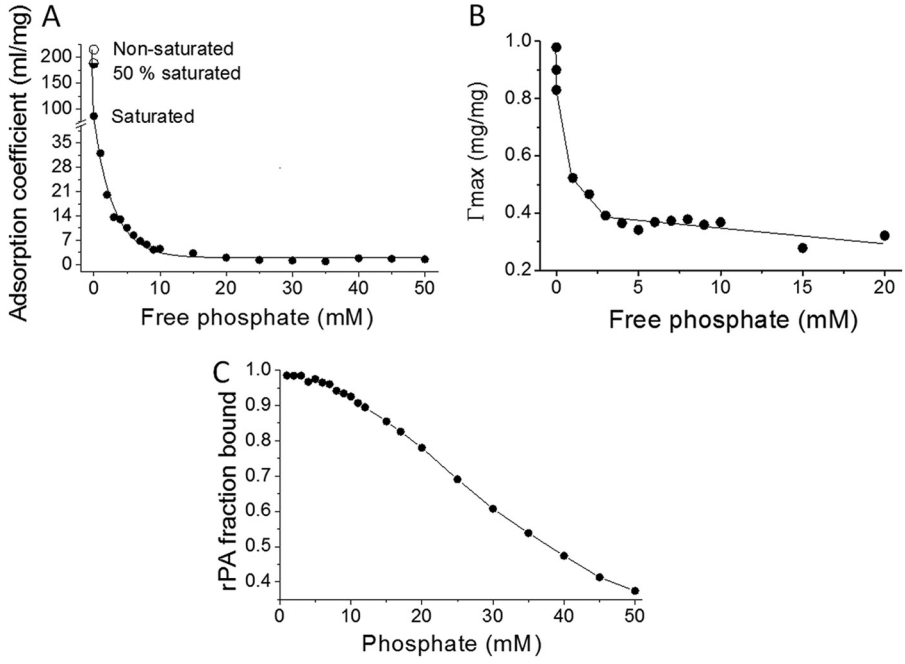

FIG 2 Results from linear regression fit to the Langmuir adsorption isotherm, showing the effects of phosphate on the adsorption coefficient (A), the binding capacity of Alhydrogel for rPA (B), and the fraction of rPA binding to Alhydrogel (C) in samples of 200 μg/ml rPA and 2.6 mg/ml Alhydrogel.

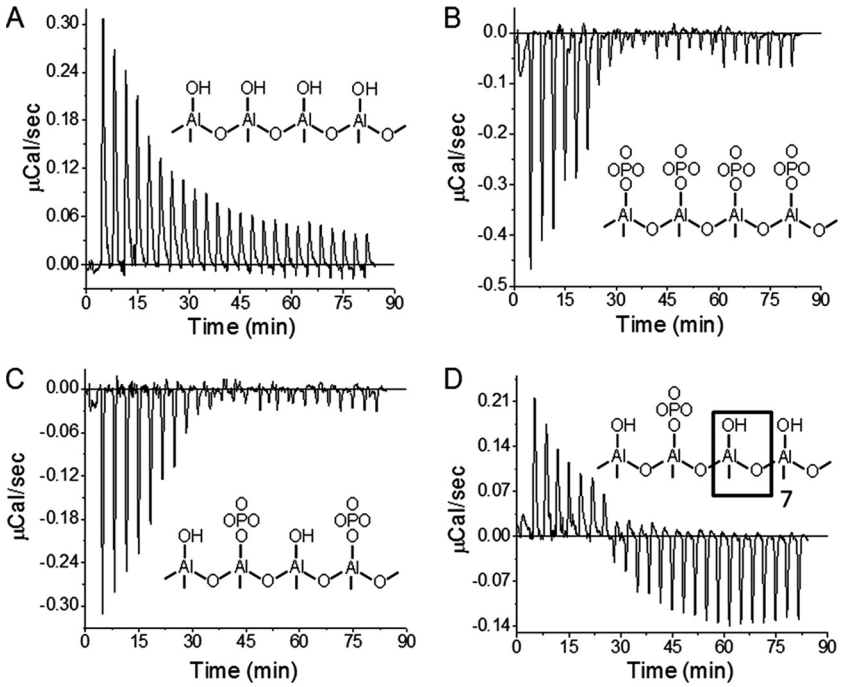

FIG 4 Titration of Alhydrogel with rPA, showing thermograms for nonmodified Alhydrogel (A), 100% phosphate-saturated Alhydrogel (B), 50% phosphate-saturated Alhydrogel (C), and 10% phosphate-saturated Alhydrogel (D). (Insets) Diagrams showing the likely surface chemistry of the variously saturated adjuvants.

nonmodified Alhydrogel with rPA gave a series of endothermic peaks (Fig. 4A), whose magnitude decreased gradually through the titration due to a decrease of free binding sites on Alhydrogel. In stark contrast, the binding of rPA to phosphate-saturated Alhydrogel was exothermic, and the adjuvant was more rapidly saturated with the protein, implying that fewer binding sites were available (Fig. 4B). Similarly, titration of 50% phosphate-saturated Alhydrogel was exothermic but the magnitude was less than that of phosphate-saturated Alhydrogel (Fig. 4C). A complex result was observed with 10% phosphate-saturated Alhydrogel, which presumably presents mixed binding surfaces to the rPA. The interaction was endothermic at the beginning of titration but gradually changed to exothermic (Fig. 4D), suggesting that the initial entropy-driven interaction with AlOH was preferred over the subsequent enthalpy-driven binding to phosphate-modified surfaces.

Solid-state circular dichroism. The solid-state (31, 34) far-UV CD spectra of rPA-AlOH closely resembled those of soluble rPA (35) (Fig. 5A), indicating minimal secondary structure perturbation upon binding to Alhydrogel. Increasing phosphate concentrations did not significantly affect the spectra. The near-UV solid-state CD spectra of rPA-AlOH at 0.25 mM phosphate, 4 mM phosphate, and 10 mM phosphate were also similar, with each showing the two prominent positive CD bands for tryptophan at 284 nm and 291 nm. These two bands, which are characteristic of rPA (31, 35), were weaker than for soluble rPA in solution (Fig. 5B); in the 10 mM phosphate sample, two bands (272 nm and 276 nm) that were not present for soluble rPA were observed. In the

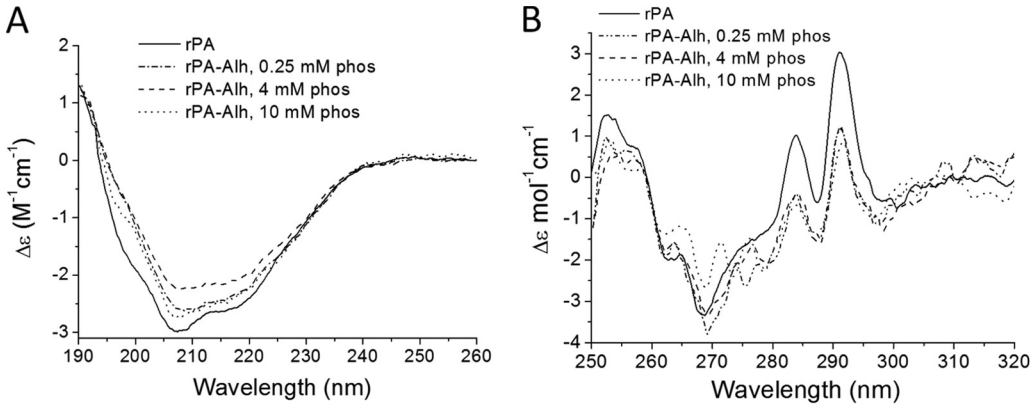

FIG 5 Effects of phosphate (phos) on solid-state circular dichroism of 200 μg/ml rPA with 2.6 mg/ml Alhydrogel (Alh). (A) Far-UV CD spectra. (B) Near-UV CD spectra.

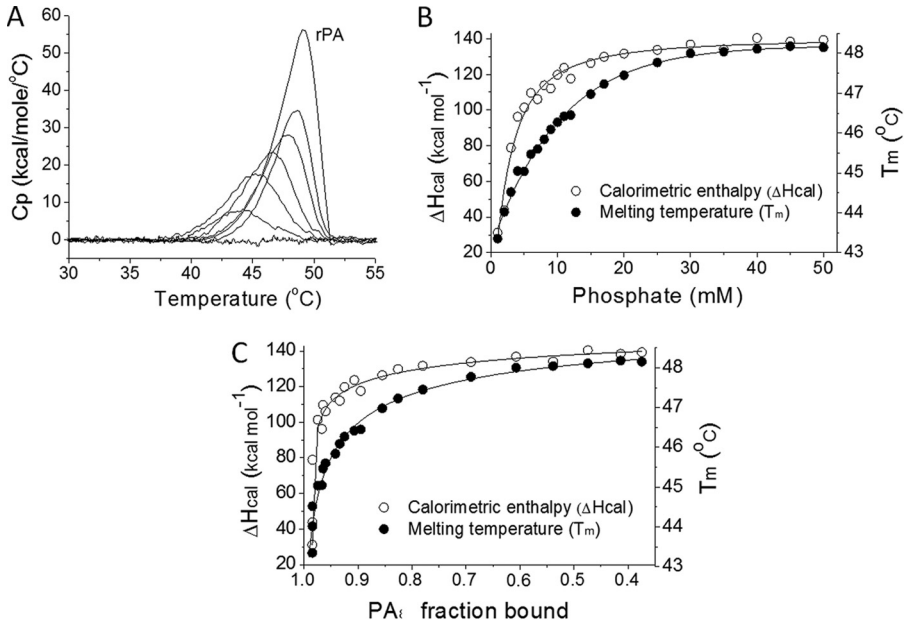

FIG 6 Phosphate effects on the structure and stability of adjuvanted rPA. (A) Overlay showing direct scanning calorimetry endotherms of rPA on Alhydrogel in 0, 2, 5, 10, 20, and 45 mM phosphate and rPA without adjuvant. Cp, heat capacity. (B) T_m and ΔH_{cal} values as functions of the phosphate concentration. (C) T_m and ΔH_{cal} changes according to the fraction of bound rPA. Samples contained 0.3 mg/ml rPA and 3 mg/ml phosphate-saturated Alhydrogel.

phenylalanine region, a broad positive band from 250 to 260 nm was seen for soluble rPA, which sharpened when rPA was bound to Alhydrogel, irrespective of the phosphate concentration. Thus, the phosphate modification of the Alhydrogel interaction has clear but subtle effects on the tertiary structure of rPA.

Differential scanning calorimetry. The transition temperature (T_m) and calorimetric enthalpy (ΔH_{cal}) of rPA are strongly affected by binding to Alhydrogel (18, 23). Surprisingly, the protein had no measurable melting transition when it was adsorbed to nonmodified or phosphate-saturated Alhydrogel. However, as the free phosphate concentration increased, there appeared to be a distinct thermal transition that eventually resembled the behavior of free rPA (Fig. 6A). Between 1 and 50 mM phosphate, the T_m rose from 43.3°C to 48.2°C and the ΔH_{cal} increased from 31 kcal mol^{-1} to 139 kcal mol^{-1} (Fig. 6B). The T_m and ΔH_{cal} of nonadjuvanted rPA protein were 49.2°C and 219 kcal mol^{-1}, respectively. Plotting T_m and ΔH_{cal} values against the fraction of bound protein revealed that these changes in thermodynamic parameters took place when >90% of rPA was still bound to Alhydrogel (Fig. 6C). Conversely, above 10 mM phosphate, when protein binding was less than 90% (Fig. 2C), there were only minor changes in T_m and ΔH_{cal}. The phosphate concentration range in which major thermodynamic changes occurred was 1 to 10 mM, at which the majority of the rPA was in the bound form.

Tryptophan fluorescence. The tryptophan emission spectrum of rPA on Alhydrogel was similar to that of free rPA, irrespective of phosphate concentration (see the supplemental material). All spectra exhibited maxima near 330 nm and had the same barycentric mean values of 340.6 ± 0.1 nm (18). The tryptophan emission spectrum of rPA on Alhydrogel had weaker intensity than the emission spectrum of rPA without adjuvant, likely due to inhomogeneous distribution of fluorophores in solution, the colloidal nature of the sample, and light scattering. Overall, these data demonstrate no measurable changes in the protein tertiary structure due to phosphate (see the supplemental material).

Protein unfolding was monitored by tryptophan fluorescence while the temperature was increased from 25°C to 65°C at the rate of 1°C min^{-1} (18). In samples containing nonmodified and 50% and 100% phosphate-saturated Alhydrogel, the protein had no distinct unfolding transition and exhibited only small changes in fluorescence, most of which were due to the quenching effects of higher temperatures (Fig. 7A). However, with free phosphate (i.e., around 2.6 mM), rPA had a well-defined transition region between 40°C and 50°C (Fig. 7B). It should be noted that increasing phosphate concentrations shifted the transition midpoint from 43.5°C to 48.0°C, compared to the 48.5°C transition temperature of nonadjuvanted rPA. It should also be noted that, in 10 mM phosphate, nearly 90% of rPA was bound to Alhydrogel.

Measurements of potency and stability. For practical and ethical reasons, the study of the effects of phosphate ions on the potency of the rPA-AlOH formulation used only two formulations, namely, 0.25 mM and 4 mM phosphate rPA-AlOH. The 0.25 mM phosphate rPA-AlOH represented an unsaturated formulation in which the Alhydrogel retained surface hydroxyl groups, whereas the 4 mM phosphate rPA-AlOH represented phosphate-saturated Alhydrogel plus free/excess phosphate. The average pH values of the bulk solutions were 6.0 ± 0.3 ($n = 4$) and 7.1 ± 0.1 ($n = 7$) for the 0.25 mM and 4 mM phosphate rPA-AlOH formulations, respectively.

Potency was determined using the mouse anthrax challenge assay, evaluating several batches of these two formulation prototypes immediately following manufacture. For each potency analysis, a 4-fold dilution curve was determined. The ED_{50} values were estimated by fitting a survival analysis model to the results of the potency assay, using a model that assumes that the survival times have a log-normal distribution and that there is a linear relation-

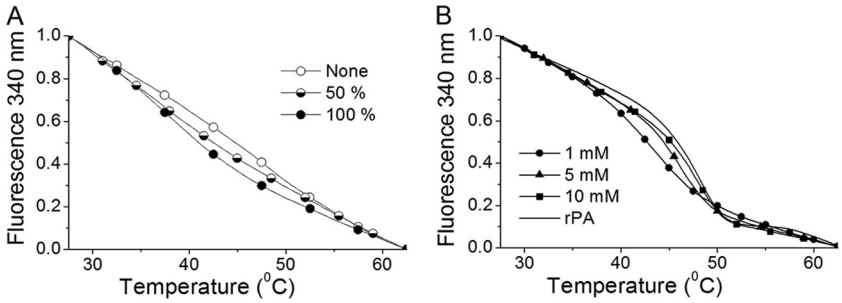

FIG 7 Tryptophan fluorescence and thermal denaturation of rPA bound to Alhydrogel. (A) rPA adsorbed to nonmodified and 50% and 100% phosphate-saturated Alhydrogel. (B) rPA on Alhydrogel with 1 to 10 mM free phosphate. The thermal transition of nonadjuvanted rPA (solid line) occurred at 48.5°C. All curves were normalized to values of 1 at 25°C and 0 at 65°C.

ship between log dose and log survival time (Table 1) (36). It should be noted that, for three of the 4 mM phosphate rPA-AlOH batches, more than one measurement of ED_{50} was taken at release and these data have been incorporated into the statistical analysis. The weighted mean ED_{50} for the 0.25 mM phosphate rPA-AlOH batches was 0.21 μg/0.1 ml (back-transformed from the mean $\log_{10}ED_{50}$ value of −0.679), whereas the value for 4 mM phosphate rPA-AlOH was 0.04 μg/0.1 ml (mean $\log_{10}ED_{50}$ value of −1.398). The weighted mean was used (weighted by the inverse of the variance of the $\log_{10}ED_{50}$) to down-weight less-precise $\log_{10}ED_{50}$ estimates. Statistical analysis using analysis of variance (ANOVA) indicated that, at release, 4 mM phosphate rPA-AlOH was significantly more potent than 0.25 mM phosphate rPA-AlOH, as shown by a difference in $\log ED_{50}$ values ($P = 0.006$). The ANOVA took batch and operator into account. Comparison of the mean ED_{50} values indicated that the 4 mM phosphate rPA-AlOH formulation was 5.25-fold more potent than the 0.25 mM phosphate formulation.

TABLE 1 Summary of potency data at release for 0.25 mM phosphate and 4 mM phosphate in final rPA-AlOH drug product

Material type	Batch no.	n^b	$\log ED_{50}$	$\log ED_{50}$ SD	ED_{50} (μg/0.1 ml)
0.25 mM phosphate FDP[a]	1	1	−0.130	0.285	
	2	1	−1.681	0.514	
	3	1	−0.484	0.193	
	4	1	−1.338	0.288	
Weighted mean					0.21
4 mM phosphate FDP	5	1	−2.202	0.789	
	6	4	−1.133	0.154	
			−1.367	0.229	
			−1.862	0.248	
			−1.273	0.159	
	7	4	−1.420	0.129	
			−1.640	1.117	
			−1.605	0.220	
			−1.451	0.203	
	8	1	0.348	0.594	
	9	2	−0.505	0.241	
			−1.419	0.242	
	10	1	−1.175	0.235	
	11	1	−1.397	0.265	
Weighted mean					0.04

[a] FDP, final drug product.
[b] An *n* value of 1 means 1 test item comprising a 4-point dilution series with 15 mice/dose and compared to the reference standard. On some occasions, the analysis was repeated up to 4 times to test reproducibility.

In addition, long-term, real-time stability studies were performed with a batch of 0.25 mM phosphate rPA-AlOH and a batch of 4 mM phosphate rPA-AlOH. In accordance with International Conference on Harmonisation guideline Q1A(R2) (37), the materials were stored for at least 3 years at 2 to 8°C under controlled conditions, which were monitored to ensure temperature compliance. During the 3 years of storage, samples were analyzed for potency using the mouse anthrax challenge assay. Trending analysis was performed after 3 years to determine the overall stability of the two vaccine formulations, and the data are presented in Fig. 8.

Linear regression analysis of data for the 0.25 mM phosphate rPA-AlOH formulation after 39 months of storage at 2 to 8°C revealed no evidence of an increase in $\log ED_{50}$ values after manufacture (intercept = −0.414 [ED_{50} = 0.385]; slope = 0.007; P = 0.480). Similarly, the 4 mM phosphate rPA-AlOH formulation exhibited no evidence of a significant increase in $\log ED_{50}$ after 36 months of storage at 2 to 8°C (intercept = −1.277 [ED_{50} = 0.0528]; slope = 0.007; P = 0.673). Trending analysis was also performed with three batches of the 4 mM phosphate rPA-AlOH formulation, to provide supporting data on stability. Using relative potency versus a freshly formulated rPA-AlOH standard, the rPA-AlOH formulation was shown to be stable for at least 37 months (see the supplemental material).

DISCUSSION

Aluminum-based adjuvants are used extensively in the formulation of a range of vaccine types, including subunit vaccines, being both effective in boosting immune responses and safe for use in humans (14). Although mainly used against infectious diseases, they are also effective in anticancer vaccines (38). Aluminum oxyhydroxide formulations, such as Alhydrogel, are the most commonly used since they are positively charged at physiological pH and bind most antigens, which tend to be acidic. A significant feature of aluminum oxyhydroxide chemistry is the ligand-exchange reaction, whereby surface hydroxyl groups are readily exchanged for phosphate ions (26). Consequently, the surface layer of the aluminum oxyhydroxide is converted to aluminum phosphate, which radically changes the surface charge properties of the Alhydrogel particles. Consequently, we performed a series of studies to explore how phosphate modification of Alhydrogel (27) affects the properties of the vaccine. Upon mixing, phosphate ions rapidly bound to Alhydrogel particles until a saturation point was

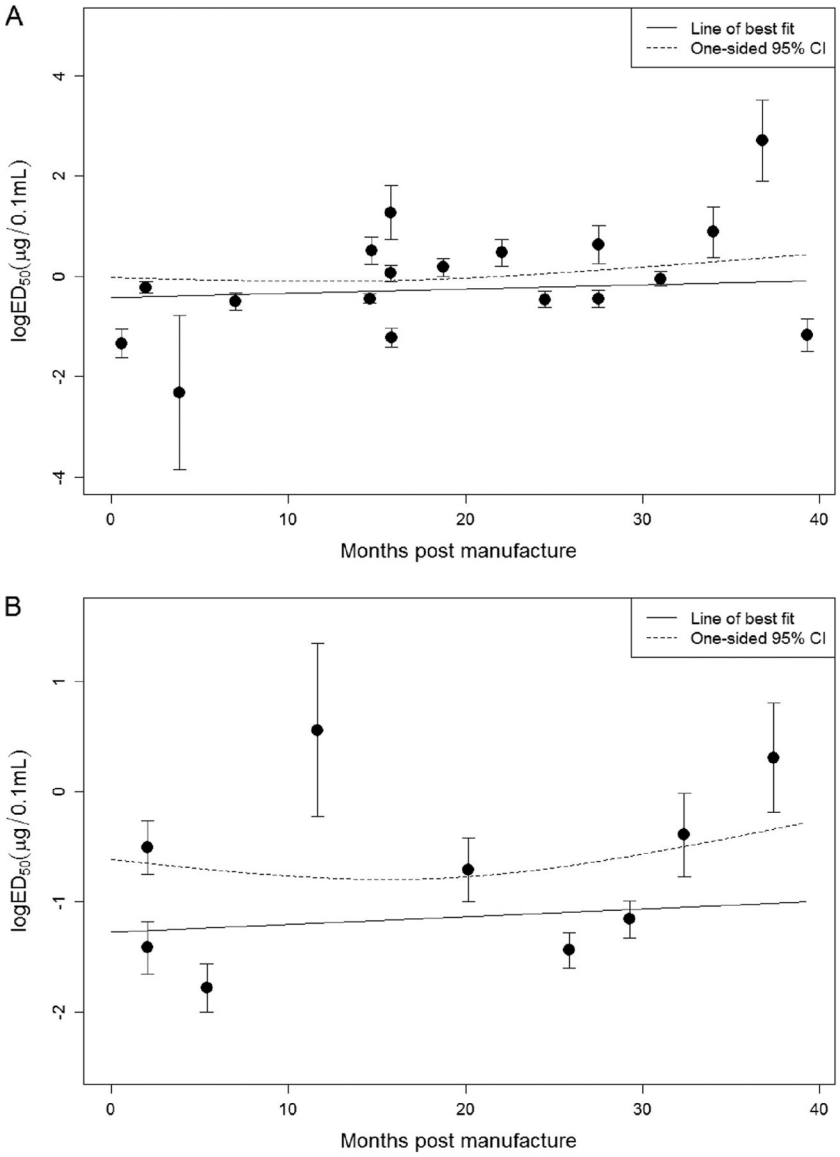

FIG 8 Stability of $logED_{50}$ for rPA-AlOH with 0.25 mM phosphate (A) and rPA-AlOH with 4 mM phosphate (B), both stored at 2 to 8°C. Error bars, standard deviation; solid line, trending line; dashed line, one-sided 95% confidence interval (CI).

reached, with 0.43 μmol phosphate saturating 12.8 μmol (1 mg) of Alhydrogel. Since there are 2 mol of hydroxyl groups per 1 mol of Alhydrogel, the theoretical maximum for phosphate saturation requires 12.8 × 2 (i.e., 25.6) μmol phosphate. Thus, we assume that only 1.7% of potential reactive groups were on the surface and available for phosphate binding. This confirms that the majority of the hydroxyl groups are not exposed on the surface but are contained within the colloidal particle itself (21).

Despite the reversal in surface charge (Fig. 3), it was surprising that, even with supersaturating concentrations of phosphate, the acidic rPA protein at the formulation density of 200 μg per 2.6 mg of AlOH was still predominantly bound (>90%) to the Alhydrogel particles (Fig. 3). One possible explanation might be the variety of charged groups on rPA. Although acidic, with a pI of 5.6, rPA contains 85 cationic (Arg plus Lys) versus 96 anionic (Asp plus Glu) side chains, and the former may be sufficient to bind to the negatively charged phosphate groups in a more selective manner. The effects of increasing phosphate concentrations extended beyond the point of surface saturation, which suggests that the surface charge of the Alhydrogel is not determined purely by the extent of ligand exchange. There is thus also a role for free phosphate in modulating the interactions between the rPA and the Alhydrogel surface.

On native Alhydrogel, the interaction of rPA with the hydroxyl groups was endothermic, meaning that it was driven by an increase in entropy, an effect often attributed to dehydration effects. This would imply that there is a significant reduction of the water-accessible surface upon rPA binding (39, 40). In contrast, above the point of phosphate saturation, the reaction became exothermic and was no longer driven solely by entropy. This enthalpy-favored interaction could be associated with the formation of direct noncovalent bonds at the particle surface. At subsaturating phosphate concentrations, the thermodynamics are complex; at 10% saturation, there is evidence for a

genuinely mixed surface offering high-affinity (endothermic) and low-affinity (exothermic) sites.

On phosphate-saturated Alhydrogel, cooperative thermal unfolding (18, 23) was more evident and became increasingly pronounced with increased free phosphate, although the protein was still bound to the Alhydrogel. With increasing phosphate concentrations, surface-bound proteins thus appear to increasingly behave as though in solution. Thus, enhanced hydration (41) could explain both the ITC data and the increased protein thermostability.

Of paramount importance are the role of phosphate in the potency of the rPA subunit vaccine and its stability when stored under refrigeration. The phosphate-subsaturated 0.25 mM phosphate rPA-AlOH formulation was significantly less potent than the 4 mM phosphate rPA-AlOH formulation, and one contrasting feature of the two formulations was the pH of the bulk solution, with the 0.25 mM phosphate rPA-AlOH formulation having a pH of 5.9 and the 4 mM phosphate rPA-AlOH formulation a value of around 7.1. Consequently, the differing bulk solution pH values might explain the differences in ED_{50} values, particularly since rPA is acid labile (35, 42). However, the biophysical analysis of the protein structure of rPA-AlOH under low-phosphate conditions does not support any major acid-induced transformation of the protein structure (31, 35). Furthermore, with 0.25 mM phosphate rPA-AlOH, the Alhydrogel surface and bound antigen would have a local pH approximately 2 units higher, due to the positive surface charge attracting hydroxyl anions (27). In contrast, the negatively charged phosphate-saturated Alhydrogel would be expected to attract protons and hence have a more acidic microenvironment than the bulk solution.

Hansen and coworkers have hypothesized that the immunogenic response to an aluminum-adjuvanted protein antigen is inversely related to the adsorption coefficient (10). They and others have also shown that antigens can be rapidly released from the Alhydrogel depot, suggesting that the directly interacting adjuvant and antigen do not stimulate the immune response (11, 13, 43). Consequently, the ability of phosphate to modulate the adsorption coefficient of an acidic protein antigen and aluminum oxyhydroxide adjuvants might appear to be irrelevant. However, enhanced immunogenicity was seen when a recombinant *Candida* antigen (rAls3p-N) was diluted with phosphate-buffered saline versus saline alone (44). Similarly, phosphate modulation of aluminum oxyhydroxide in both hepatitis B surface antigen and HIV-1 (SF162dV2gp140) subunit vaccines demonstrated enhancement of immunogenicity (8, 9).

There have been several proposed mechanisms of action for aluminum-containing adjuvants, including acting as a depot in tissues to produce prolonged exposure (45), enhanced delivery of antigen to antigen-presenting cells (46), induction of uric acid for activation of inflammatory dendritic cells (47), and enhanced proteolytic processing by the immune system due to destabilization of the antigen structure (23). However, compelling evidence has recently been produced to demonstrate that aluminum-containing adjuvants have direct effects on dendritic cells (6, 7, 48). Certainly a weakly bound antigen, as found in phosphate-saturated Alhydrogel, would be more likely to be internalized and processed by dendritic cells. It should be noted that the physiological level of phosphate is strictly regulated at 0.8 to 1.4 mM (49). Upon injection into this phosphate concentration, exposed surface hydroxyl groups are likely to be replaced, and if it is not saturated with phosphate already, the aluminum oxyhydroxide will be saturated following injection. Surprisingly, our data show that the difference between the 0.25 mM phosphate rPA-AlOH and 4 mM phosphate rPA-AlOH formulations persists. It is possible that binding of the rPA to the Alhydrogel under subsaturating conditions occludes hydroxyl groups and prevents subsequent phosphate exchange. Under such circumstances, the stronger binding conditions may prevail even with later exposure to physiological phosphate concentrations Although Iyer et al. showed that aluminum adjuvant interactions with a basic protein (lysozyme) could be reversed in interstitial fluid, this was true only for freshly formulated mixtures of acidic ovalbumin, and older samples did not release antigen (50). Thus, if both rPA (pI 5.6) and ovalbumin (pI 4.7) rearrange slowly on the adjuvant surface, then the effect of phosphate we observe may be indefinite maintenance of the loose interaction state.

Overall, the results are consistent with previous data showing that phosphate is a beneficial modulating agent for rPA binding to Alhydrogel. This study goes much further, however, in clarifying the role of phosphate, which could be explained by weaker interactions allowing a more complete water layer to be formed between the protein and the adjuvant. Thus, the hypothesis of Hansen and coworkers that the immunogenic response to an aluminum-adjuvanted protein antigen is inversely related to the adsorption coefficient (10) is strongly confirmed but also is extended to include the physical effects on the protein and the effects on potency over a long period. Combined with recent data indicating that some adjuvant-protein interactions rapidly dissociate upon injection (13), it appears that the strongest aluminum adjuvant effects are likely to be via weakly attached or easily released native-state antigen proteins.

ACKNOWLEDGMENTS

We thank D. Woodhouse for performing the zeta potential analysis. Additionally, we thank N. C. Price and S. Kelly, University of Glasgow, for providing access to the CD facility, Margaret Nutley for technical assistance, and Barry Moore for discussions on the CD data.

This work was supported in part by NIAID challenge grant award 1UC1AI67223-01, NIAID contracts N01-AI-25492 and N01-AI-30052, and BARDA contract HHSO100200900103C. Allan Watkinson, Karie Hirst, Peter C. Fusco, and Thomas R. Fuerst received compensation from PharmAthene as employees and consultants during the conduct of these studies and manuscript preparation. The work carried out by Andrei Soliakov and Jeremy H. Lakey was partly funded by PharmAthene.

REFERENCES

1. **Liljeqvist S, Stahl S.** 1999. Production of recombinant subunit vaccines: protein immunogens, live delivery systems and nucleic acid vaccines. J. Biotechnol. **73:**1–33.
2. **Petosa C, Collier JR, Klimpel KR, Leppla SH, Liddington RC.** 1997. Crystal structure of the anthrax toxin protective antigen. Nature **385:**833–838.
3. **Perrie Y, Mohammed AR, Kirby DJ, McNeil SE, Bramwell VW.** 2008. Vaccine adjuvant systems: enhancing the efficacy of sub-unit protein antigens. Int. J. Pharm. **364:**272–280.
4. **Rinella JV, White JL, Hem SL.** 1996. Treatment of aluminium hydroxide adjuvant to optimize the adsorption of basic proteins. Vaccine **14:**298–300.
5. **Glenny AT, Pope CG, Waddington H, Wallace U.** 1926. Immunology notes. XXIII. The antigenic value of toxoid precipitated by potassium alum. J. Pathol. Bacteriol. **29:**31–40.
6. **Flach TL, Ng G, Hari A, Desrosiers MD, Zhang P, Ward SM, Seamone ME, Vilaysane A, Mucsi AD, Fong Y, Prenner E, Ling CC, Tschopp J, Muruve DA, Amrein MW, Shi Y.** 2011. Alum interaction with dendritic

cell membrane lipids is essential for its adjuvanticity. Nat. Med. **17:**479–487.
7. **Levitz SM, Golenbock DT.** 2012. Beyond empiricism: informing vaccine development through innate immunity research. Cell **148:**1284–1292.
8. **Hansen B, Malyala P, Singh M, Sun Y, Srivastava I, Hogenesch H, Hem SL.** 2011. Effect of the strength of adsorption of HIV 1 SF162dV2gp140 to aluminum-containing adjuvants on the immune response. J. Pharm. Sci. **100:**3245–3250.
9. **Hansen B, Belfast M, Soung G, Song L, Egan PM, Capen R, HogenEsch H, Mancinelli R, Hem SL.** 2009. Effect of the strength of adsorption of hepatitis B surface antigen to aluminum hydroxide adjuvant on the immune response. Vaccine **27:**888–892.
10. **Hansen B, Sokolovska A, HogenEsch H, Hem SL.** 2007. Relationship between the strength of antigen adsorption to an aluminum-containing adjuvant and the immune response. Vaccine **25:**6618–6624.
11. **Romero Mendez IZ, Shi Y, HogenEsch H, Hem SL.** 2007. Potentiation of the immune response to non-adsorbed antigens by aluminum-containing adjuvants. Vaccine **25:**825–833.
12. **Jiang DP, Morefield GL, HogenEsch H, Hem SL.** 2006. Relationship of adsorption mechanism of antigens by aluminum-containing adjuvants to in vitro elution in interstitial fluid. Vaccine **24:**1665–1669.
13. **Hutchison S, Benson RA, Gibson VB, Pollock AH, Garside P, Brewer JM.** 2012. Antigen depot is not required for alum adjuvanticity. FASEB J. **26:**1272–1279.
14. **Shirodkar S, Hutchinson RL, Perry DL, White JL, Hem SL.** 1990. Aluminum compounds used as adjuvants in vaccines. Pharm. Res. **7:**1282–1288.
15. **Bruhne S, Gottlieb S, Assmus W, Alig E, Schmidt MU.** 2008. Atomic structure analysis of nanocrystalline boehmite AlO(OH). Crystal Growth Design **8:**489–493.
16. **Yau PK, Schulze DG, Johnston CT, Hem SL.** 2006. Aluminum hydroxide adjuvant produced under constant reactant concentration. J. Pharm. Sci. **95:**1822–1833.
17. **Seeber S, White JJL, Hem SL.** 1991. Predicting the adsorption of proteins by aluminium-containing adjuvants. Vaccine **9:**201–203.
18. **Soliakov A, Kelly IF, Lakey JH, Watkinson A.** 2012. Anthrax sub-unit vaccine: the structural consequences of binding rPA83 to Alhydrogel^{R}. Eur. J. Pharm. Biopharm. **80:**25–32.
19. **Agopian A, Ronzon F, Sauzeat E, Sodoyer R, El Habib R, Buchet R, Chevalier M.** 2007. Secondary structure analysis of HIV-1-gp41 in solution and adsorbed to aluminum hydroxide by Fourier transform infrared spectroscopy. Biochim. Biophys. Acta **1774:**351–358.
20. **Dong A, Jones LS, Kerwin BA, Krishnan S, Carpenter JF.** 2006. Secondary structures of proteins adsorbed onto aluminum hydroxide: infrared spectroscopic analysis of proteins from low solution concentrations. Anal. Biochem. **351:**282–289.
21. **Harris JR, Soliakov A, Lewis RJ, Depoix F, Watkinson A, Lakey JH.** 2012. Alhydrogel^{R} adjuvant, ultrasonic dispersion and protein binding: a TEM and analytical study. Micron **43:**192–200.
22. **Soliakov A, Harris JR, Watkinson A, Lakey JH.** 2010. The structure of *Yersinia pestis* Caf1 polymer in free and adjuvant bound states. Vaccine **28:**5746–5754.
23. **Jones LS, Peek LJ, Power J, Markham A, Yazzie B, Middaugh CR.** 2005. Effects of adsorption to aluminum salt adjuvants on the structure and stability of model protein antigens. J. Biol. Chem. **280:**13406–13414.
24. **Peek LJ, Martin TT, Nation CE, Pegram SA, Middaugh CR.** 2007. Effects of stabilizers on the destabilization of proteins upon adsorption to aluminum salt adjuvants. J. Pharm. Sci. **96:**547–557.
25. **Morefield GL, HogenEsch H, Robinson JP, Hem SL.** 2004. Distribution of adsorbed antigen in mono-valent and combination vaccines. Vaccine **22:**1973–1984.
26. **Hem SL, HogenEsch H.** 2007. Relationship between physical and chemical properties of aluminum-containing adjuvants and immunopotentiation. Expert Rev. Vaccines **6:**685–698.
27. **Wittayanukulluk A, Jiang DP, Regnier FE, Hem SL.** 2004. Effect of microenvironment pH of aluminum hydroxide adjuvant on the chemical stability of adsorbed antigen. Vaccine **22:**1172–1176.
28. **Williamson ED, Hodgson I, Walker NJ, Topping AW, Duchars MG, Mott JM, Estep J, LeButt C, Flick-Smith HC, Jones HE, Li H, Quinn CP.** 2005. Immunogenicity of recombinant protective antigen and efficacy against aerosol challenge with anthrax. Infect. Immun. **73:**5978–5987.
29. **Langmuir I.** 1916. The constitution and fundamental properties of solids and liquids: part 1: solids. J. Am. Chem. Soc. **38:**2221–2295.
30. **Bustamante C, Maestre MF.** 1988. Statistical effects in the absorption and optical activity of particulate suspensions. Proc. Natl. Acad. Sci. U. S. A. **85:**8482–8486.
31. **Ganesan A, Watkinson A, Moore BD.** 2012. Biophysical characterisation of thermal-induced precipitates of recombinant anthrax protective antigen: evidence for kinetically trapped unfolding domains in solid-state. Eur. J. Pharm. Biopharm. **82:**475–484.
32. **Lakey JH, Magetdana R, Ptak M.** 1989. The lipopeptide antibiotic A21978C has a specific interaction with DMPC only in the presence of calcium-ions. Biochim. Biophys. Acta **985:**60–66.
33. **Lindblad EB.** 2004. Aluminium compounds for use in vaccines. Immunol. Cell Biol. **82:**497–505.
34. **Ganesan A, Lyle C, Halling PJ, Kelly S, Price N, Moore BD.** 2006. Assessing the structure of immobilised proteins and antigens using circular dichroism. J. Pharm. Pharmacol. **58:**9.
35. **Chalton DA, Kelly IF, McGregor A, Ridley H, Watkinson A, Miller J, Lakey JH.** 2007. Unfolding transitions of *Bacillus anthracis* protective antigen. Arch. Biochem. Biophys. **465:**1–10.
36. **Collett D.** 2003. Modelling survival data in medical research, 2nd ed. CRC Press, Boca Raton, FL.
37. **Food and Drug Administration.** 2004. International Conference on Harmonisation: evaluation of stability data: availability: notice. Fed. Regist. **69:**32010–32011.
38. **Hamid O, Solomon JC, Scotland R, Garcia M, Sian S, Ye W, Groshen SL, Weber JS.** 2007. Alum with interleukin-12 augments immunity to a melanoma peptide vaccine: correlation with time to relapse in patients with resected high-risk disease. Clin. Cancer Res. **13:**215–222.
39. **Cooper A, Johnson CM, Lakey JH, Nollmann M.** 2001. Heat does not come in different colours: entropy-enthalpy compensation, free energy windows, quantum confinement, pressure perturbation calorimetry, solvation and the multiple causes of heat capacity effects in biomolecular interactions. Biophys. Chem. **93:**215–230.
40. **Jelesarov I, Bosshard HR.** 1999. Isothermal titration calorimetry and differential scanning calorimetry as complementary tools to investigate the energetics of biomolecular recognition. J. Mol. Recognit. **12:**3–18.
41. **Svergun DI, Richard S, Koch MHJ, Sayers Z, Kuprin S, Zaccai G.** 1998. Protein hydration in solution: experimental observation by x-ray and neutron scattering. Proc. Natl. Acad. Sci. U. S. A. **95:**2267–2272.
42. **Young JAT, Collier RJ.** 2007. Anthrax toxin: receptor binding, internalization, pore formation, and translocation. Annu. Rev. Biochem. **76:**243–265.
43. **Noe SM, Green MA, HogenEsch H, Hem SL.** 2010. Mechanism of immunopotentiation by aluminum-containing adjuvants elucidated by the relationship between antigen retention at the inoculation site and the immune response. Vaccine **28:**3588–3594.
44. **Lin L, Ibrahim AS, Avanesian V, Edwards JE, Fu Y, Baquir B, Taub R, Spellberg B.** 2008. Considerable differences in vaccine immunogenicities and efficacies related to the diluent used for aluminum hydroxide adjuvant. Clin. Vaccine Immunol. **15:**582–584.
45. **Hunter RL.** 2002. Overview of vaccine adjuvants: present and future. Vaccine **20**(Suppl 3)**:**S7–S12.
46. **Brewer JM, Pollock KGJ, Tetley L, Russell DG.** 2004. Vesicle size influences the trafficking, processing, and presentation of antigens in lipid vesicles. J. Immunol. **173:**6143–6150.
47. **Kool M, Soullie T, van Nimwegen M, Willart MAM, Muskens F, Jung S, Hoogsteden HC, Hammad H, Lambrecht BN.** 2008. Alum adjuvant boosts adaptive immunity by inducing uric acid and activating inflammatory dendritic cells. J. Exp. Med. **205:**869–882.
48. **Kuroda E, Ishii KJ, Uematsu S, Ohata K, Coban C, Akira S, Aritake K, Urade Y, Morimoto Y.** 2011. Silica crystals and aluminum salts regulate the production of prostaglandin in macrophages via NALP3 inflammasome-independent mechanisms. Immunity **34:**514–526.
49. **Keele C, Neil E, Joels N.** 1984. Samson Wright's applied physiology, 13th ed. Oxford Medical Publications, Oxford, England.
50. **Iyer S, HogenEsch H, Hem SL.** 2003. Relationship between the degree of antigen adsorption to aluminum hydroxide adjuvant in interstitial fluid and antibody production. Vaccine **21:**1219–1223.
51. **Bencini DA, Wild JR, O'Donovan GA.** 1983. Linear one-step assay for the determination of orthophosphate. Anal. Biochem. **132:**254–258.